ARTICLE OPEN

Check for updates

Infinite-layer nickelates as Ni-e_g Hund's metals

Byungkyun Kang[1], Corey Melnick[1], Patrick Semon[1], Siheon Ryee[2], Myung Joon Han[2], Gabriel Kotliar[1,3] and Sangkook Choi[1,4✉]

The recent and exciting discovery of superconductivity in the hole-doped infinite-layer nickelate $Nd_{1-\delta}Sr_{\delta}NiO_2$ draws strong attention to correlated quantum materials. From a theoretical view point, this class of unconventional superconducting materials provides an opportunity to unveil a physics hidden in correlated quantum materials. Here we study the temperature and doping dependence of the local spectrum as well as the charge, spin and orbital susceptibilities from first principles. By using ab initio LQSGW+DMFT methodology, we show that onsite Hund's coupling in Ni-*d* orbitals gives rise to multiple signatures of Hund's metallic phase in Ni-e_g orbitals. The proposed picture of the nickelates as an e_g (two orbital) Hund's metal differs from the picture of the Fe-based superconductors as a five orbital Hund's metal as well as the picture of the cuprates as doped charge transfer insulators. Our finding uncover a new class of the Hund's metals and has potential implications for the broad range of correlated two orbital systems away from half-filling.

npj Quantum Materials (2023)8:35 ; https://doi.org/10.1038/s41535-023-00568-5

INTRODUCTION

Although the mechanisms of unconventional superconductivity remain elusive, the discoveries of classes of unconventional superconductors have proliferated experimentally. These experimental efforts revived the interest in correlated quantum materials and provided opportunities to unveil physics hidden within them. To illustrate, in the cuprate superconductors[1], superconductivity emerges from the bad metallic states realized by doping a charge transfer insulator[2]. Strong electron correlation in the bad metallic normal states arises due to the proximity to Mott insulator transition[3,4], i.e., Mottness. According to the theory of conventional superconductors, it is improbable that this bad-metallic phase would support superconductivity. This motivated the theoretical proposals of superconducting pairing mechanisms beyond the Bardeen-Cooper-Schrieffer (BCS) paradigm[5–7]. This in turn lead to the discovery of other unconventional superconductors wherein a superconducting phase emerged from the bad-metal parent state in a different way. For example, in the multi-orbital Fe-based superconductors[8,9], the on-site Hund's coupling (J) promotes bad metallic behavior in their normal phase[10–13]. This gives rise to the concept of Hundness. Hundness-induced correlated metals, Hund's metals[14–16], play the role of a reliable reference system for Fe-based superconducting materials[12,14,15,17–21] and ruthenates[12,22–25].

Recently, the thrilling discovery of Ni-based superconductors[26–29] turns the spotlight on correlated quantum materials and their unconventional superconductivity[30,31]. $NdNiO_2$ and infinite-layer cuprates, e.g. CaCuO2, are isostructural[32,33], where the two dimensional Ni-O plane is geometrically analogous to the Cu-O plane in the cuprate. The Ni-d_{x2-y2} orbital of each Ni^{1+} ion can be expected to be half-filled with an effective spin-1/2 on each site according to the oxidation state rules. In combination, this makes $NdNiO_2$ a promising cuprate analog[34–39].

However, the differences from cuprates are striking. Its parent compound is seldom regarded as a charge transfer insulator[35,40–42] and there is no sign of long-range magnetic orders[33] down to 1.7 K. In addition, its parent compound shows a resistivity upturn upon cooling[26], which is common in heavy-fermion superconductors and is often due to Kondo effects[43,44]. The sign change of the Hall coefficient implies that electrons as well as holes may play an important role in the materials properties[26], implying its multi-orbital nature[44–46]. Moreover, it is debatable whether the doped hole forms a spin singlet or triplet doublon with the original hole on a Ni ion[47–53], suggesting possible Hund metal physics[44,44,54,55]. These similarities and differences to various unconventional superconductors are puzzling, but they do provide a chance to explore hidden aspects of electron correlation.

In this paper, we explore the multi-orbital physics in infinite-layer nickelates *from first principles*. By using ab initio linearized quasiparticle self-consistent GW (LQSGW) and dynamical mean-field theory (DMFT) method[56–58], we investigate the origin of the electron correlation in the infinite-layer nickelate normal phases. Ab initio LQSGW+DMFT is a diagrammatically motivated ab initio approaches for correlated electron systems. As a simplification of diagrammatically controlled full GW+EDMFT approach[59–61], it calculates electronic structure by using ab initio linearized quasiparticle self-consistent GW approaches[62,63]. Then it adds one-shot correction to local electron self-energy by summing over all possible local Feynmann diagrams within DMFT[64–72]. For the impurity orbital in the DMFT step, we choose a very localized orbital spanning a large energy window, which contains most strongly hybridized bands along with upper and lower Hubbard bands. Having chosen the shape of the correlated orbitals, all the other parameters to define DMFT problem are determined accordingly: double-counting energy within local GW approximation and Coulomb interaction tensor within constrained random phase approximation (cRPA)[73]. This method has been validated against various classes of correlated electron systems including paramagnetic Mott insulators La_2CuO_4[57], Hund metal FeSe[58], and correlated narrow-gap semiconductors $FeSb_2$[74]. Recently, Kondo effects of USbTe[75,76], UTe_2[77], and $NdNiO_2$[78] have been identified by this method. The calculated electronic structures well explained experimental results from ARPES and electrical resistivity measurements.

Within ab initio LQSGW+DMFT, we found multiple signatures of Hundness associated with the Ni-*d* subshell in the compounds. This finding differentiates the infinite-layer nickelates from the

[1]Condensed Matter Physics and Materials Science Department, Brookhaven National Laboratory, Upton, NY 11973, USA. [2]Department of Physics, KAIST, Daejeon 34141, Republic of Korea. [3]Department of Physics and Astronomy, Rutgers University, New Jersey, NY 08854, USA. [4]School of Computational Sciences, Korea Institute for Advanced Study, Seoul 02455, Republic of Korea. ✉email: sangkookchoi@kias.re.kr

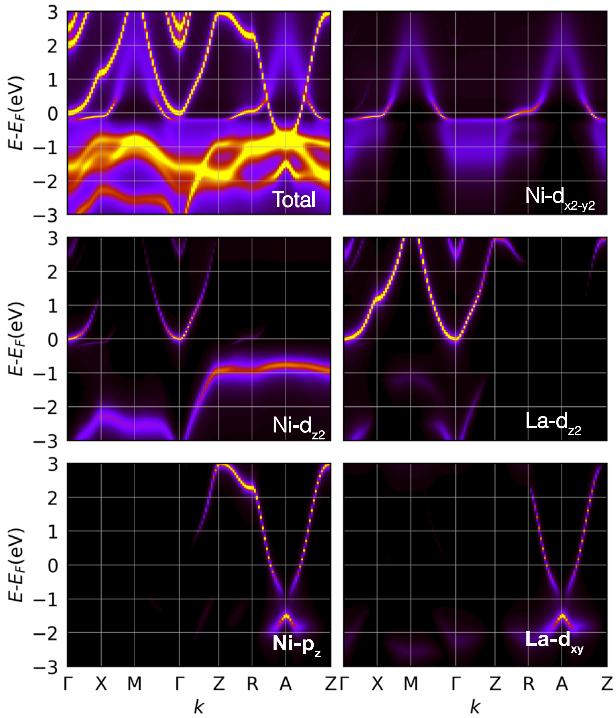

Fig. 1 Calculated spectral functions. Total and orbital-resolved spectral function of $La_{0.8}Ba_{0.2}NiO_2$ along a high-symmetry line as calculated within ab initio LQSGW+DMFT at T=300K. Of the two bands crossing the Fermi level, the lower energy band shows Ni-$d_{x^2-y^2}$ character, and the other, self-doping band at higher energy is a mixture of La-d_{z^2}, Ni-d_{z^2}, La-d_{xy} and Ni-p_z.

cuprates. In particular, we found that Hundness becomes apparent among the Ni-e_g orbitals but not the Ni-t_{2g} orbitals. This is a distinctive feature of the infinite-layer nickelates from Fe-based superconductors as five-orbital Hund's metals.

RESULTS AND DISCUSSION

Orbital-resolved spectral function

The low-energy electronic structure of $La_{1-\delta}Ba_{\delta}NiO_2$ shows multi-orbital characters. In particular, the two bands crossing the Fermi-energy have substantial Ni-e_g orbital character. Figure 1 shows the electronic structure of $La_{0.8}Ba_{0.2}NiO_2$ within ab initio LQSGW+DMFT. Consistent with the results obtained with other electronic structure methodologies such as DFT[34,37,38,43–45,53,79–85], DFT+DMFT[35,54], and one-shot G_0W_0[86], the total spectral function shows that there are two bands crossing the Fermi level. Of these two bands, the lower energy band shows strong two dimensional character, and it is dominated by the Ni-$d_{x^2-y^2}$ orbital. The remaining band, the so called self-doping band, is the higher energy band which shows strong hybridization between other Ni orbitals and La orbitals. The band dispersion of the self-doping band varies strongly along the direction normal to the Ni-O plane ($\hat{z}$), demonstrating its strong 3-dimensional character[43]. Moreover, the orbital character of the self-doping band is strongly dependent on k_z. In the k_z=0 plane, the orbital character of the self-doping band is mostly La-d_{z^2} and Ni-d_{z^2}[81,82], In contrast, in the $k_z = \pi c^{-1}$ plane, where c is the lattice constant along the $\hat{z}$ direction, its orbital character is mostly La-d_{xy} and Ni-p_z. This analysis is consistent with a recent two band model study from first-principles, showing that the two Fermi-level-crossing bands can be spanned by a Ni-$d_{x^2-y^2}$ orbital and an axial orbital[45,85,87]. The axial orbital is not centered on a single atom. Instead, its density is centered on both the Ni and La atoms.

Table 1. Electron occupation of Ni-d orbitals in $La_{0.8}Ba_{0.2}NiO_2$ and Fe-d orbitals in FeSe at T = 300 K.

Materials	d_{xy}	d_{yz}	d_{xz}	d_{z^2}	$d_{x^2-y^2}$
$La_{0.8}Ba_{0.2}NiO_2$	1.94	1.89	1.89	1.59	1.04
FeSe	1.22	1.19	1.19	1.44	1.26

Orbital occupations

Orbital occupations in the Ni-d orbitals differentiates the t_{2g} and e_g orbitals. As summarized in Table 1, the Ni-e_g orbitals are partially filled but the Ni-t_{2g} orbitals are fully-filled in $La_{0.8}Ba_{0.2}NiO_2$. This orbital occupation profile is far from a prediction based on oxidation state rules, i.e., 2, 2, 2, 2, and 1 for Ni-d_{xy}, Ni-d_{yz}, Ni-d_{xz}, Ni-d_{z^2}, and Ni-$d_{x^2-y^2}$, respectively. Intriguingly, the difference stands out especially for the Ni-z^2 orbital, which is far from the expected double occupation[55,88]. This discrepancy can be explained by the hybridization between Ni-d_{z^2} and La-d_{z^2} orbitals. The strong hybridization between these two orbitals in the Γ-X-M-Γ plane makes the Ni-d_{z^2} orbital exhibit a dispersion which is distinct from its dispersion in isolation (the flat band at E_F-1eV in the Z-R-A-Z plane in Fig. 1c)[89]. Indeed, upon Ba doping up to 0.3, only ~25% of the added holes go into the Ni-d orbitals, while the remaining holes go into other orbitals, especially the La-d_{xy}, La-d_z and Ni-p_z orbitals (as shown in the Supplementary Fig. 8). This is consistent with other theoretical studies at low-doping[54,88], and it makes the t_{2g}-e_g differentiation in orbital occupation robust against low extrinsic hole-doping. Here we note that the orbital occupation as well as the orbital resolved spectral functions are dependent on the choice of the Wannier orbitals. To construct atomic-orbital-like Wannier orbitals tightly bounded and centered on the atoms, we constructed 31 atom-centered Wannier orbitals for each spin (see the Supplementary Methods).

Coulomb interactions for Ni-d orbitals and Hund metal physics

Based on the Coulomb interaction calculation within the constrained random phase approximation (cRPA), it is legitimate to assume the dominance of Hundness over "Mottness" in $La_{1-\delta}Ba_{\delta}NiO_2$. Figure 2 shows the calculate on-site Hubbard (U) and Hund (J) interactions among five Ni-d orbitals within the constrained random phase approximation. In teteragonal nickelates, the crystal field splits the e_g into d_{z^2} and $d_{x^2-y^2}$, and the t_{2g} into d_{xy} and {d_{yz}, d_{xz}}. The calculated crystal field splitting energies are ~0.2 and ~0.4 eV for the e_g and t_{2g} orbitals, respectively. Both energies are smaller than the static $U = 2.56$ and $J = 1.09$ eV. The electronic structure of $LaNiO_2$ is affected mainly by U and J rather than the small crystal field splittings. We therefore used e_g and t_{2g} notation to describe differentiated Hund's physics among two groups of $e_g : \{d_{z^2}, d_{x^2-y^2}\}$ and t_{2g}: {d_{xy}, d_{yz}, d_{xz}}. For comparison, we plotted the U and J of Ni-d orbitals in NiO and Fe-d orbitals in FeSe. As is typical, U is strongly frequency-dependent, while J is not. Interestingly, the static U of the Ni-d orbitals in $La_{0.8}Ba_{0.2}NiO_2$ is much smaller than it is in the charge-transfer insulator NiO. It is even smaller than the U of Fe-d orbitals in the Hund's metal FeSe. In contrast, the J of the Ni-d orbitals in $La_{0.8}Ba_{0.2}NiO_2$ is even larger than the J of Fe-d in the Hund's metal FeSe. In the LQSGW approach, the crystal-field splitting between two Ni-e_g orbitals was found to be 0.2 eV, while the splitting between the Ni-d_{xy} orbital and Ni-$d_{xz/yz}$ orbital was calculated to be 0.4 eV. These values were obtained from the onsite-energy levels of atom-centered Wannier functions with the desired angular momentum characters. The crystal-field splitting energy is 0.2 (0.18) eV for d_{z^2} and $d_{x^2-y^2}$ (d_{xy} and d_{yz}) in $La_{0.8}Ba_{0.2}NiO_2$ (FeSe), which is smaller than U and J. The bandwidths are more affected by U and J than crystal-field splitting. The three Fe-d_{xy}, Fe-d_{yz}, and Ni-$d_{x^2-y^2}$ are slightly away

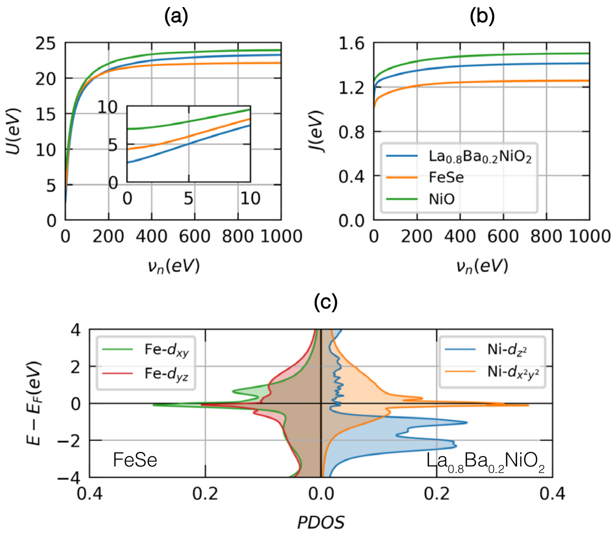

Fig. 2 Calculated onsite Coulomb interaction. **a** Calculated on-site Hubbard interaction U and **b** Hund interaction J for Ni-d orbitals in $La_{0.8}Ba_{0.2}NiO_2$, Fe-d orbitals in FeSe, and Ni-d orbitals in NiO within the constrained random phase approximation. In the static limit, the U of the Ni-d orbitals in $La_{0.8}Ba_{0.2}NiO_2$ is much smaller than in NiO and even smaller than that of the Fe-d orbitals in FeSe. In the entire frequency range, the J for Ni-d orbitals in $La_{0.8}Ba_{0.2}NiO_2$ is larger than the J of Fe-d orbitals in FeSe. **c** Projected density of states to La-e_g orbitals in $La_{0.8}Ba_{0.2}NiO_2$ and Fe-t_{2g} orbitals in FeSe.

from half filling signaling possible Hundness or Mottness. Despite significant variation on U between FeSe and $La_{0.8}Ba_{0.2}NiO_2$, bandwidths of the four orbitals are similar, we therefore can safely assume the dominant role of Hundness over Mottness in (La,Ba)NiO_2.

In FeSe, all five d orbitals are away from the nominal half-filling. This is one of the conditions leading to five orbitals Hund's metal. The nominal occupancy of Ni-d is d^9 by the oxidation state rule. However, the real occupancy of Ni-d in $LaNiO_2$ is expected to be $d^{9-\delta}$, depending on charge transfer from (to) oxygen (lanthanum) and hole doping, where $0 < \delta \ll 1$. Six electrons are occupied in the t_{2g} manifold and 3-δ electrons are occupied in the e_g manifold. This is the ideal filling for two-orbital Hund metal physics[90].

Signatures of two-orbital Hund metal physics

To understand the origin of strong correlations in the infinite-layer nickelates further, we calculated the temperature and doping dependence of Ni-$d_{x^2-y^2}$ local spectra as well as static spin- and orbital-susceptibility. These one- and two-particle quantities are "litmus-papers" to quantify the relative strength of Hundness versus Mottness. Hund's metals show various characteristic behaviors. One is spin-orbital separation: a two-step screening process in which local spin moment is screened at much lower temperature than local orbital polarization. Another is the absence of the pseudo gap in the local spectra. At high temperature when quasiparticle spectral weight near the Fermi level is transferred into high-energy Hubbard bands, spectral weight at the Fermi level is still not negligible and the local spectra is dominated by a single incoherent peak. In contrast, in the correlated metallic system where Mottness dominates, spin-orbit separation is negligible. In addition, the high-temperature spectral weight at the Fermi level is depleted due to the quasiparticle spectral weight transfer and pseudogap forms at the Fermi level at the high temperature. By calculating these quantities, we found multiple Hundness signatures. More importantly, these signatures are primarily evident in the active Ni-e_g orbitals and not the inactive Ni-t_{2g} orbitals.

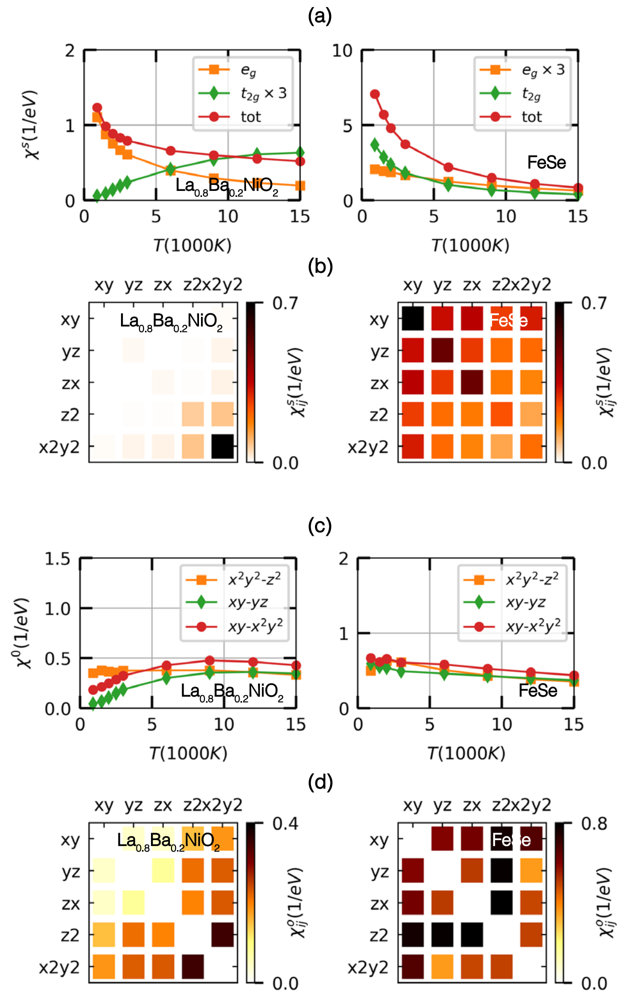

Fig. 3 The temperature dependence of the local spectrum of the spin and orbital susceptibilities. **a** The temperature dependence of static spin susceptibility (χ^s) of d orbitals (red dots), t_{2g} orbitals (green diamonds), and e_g-orbitals (orange squares) in $La_{0.8}Ba_{0.2}NiO_2$ and FeSe. **b** Orbital-resolved static spin susceptibility (χ^s_{ij}) of Ni-d orbitals in $La_{0.8}Ba_{0.2}NiO_2$ and Fe-d orbitals in FeSe at T = 900 K. **c** The temperature dependence of static orbital susceptibility (χ^o_{ij}) of Ni-d orbitals in $La_{0.8}Ba_{0.2}NiO_2$ and Fe-d orbitals in FeSe. **d** Orbital susceptibility (χ^s_{ij}) of Ni-d orbitals in $La_{0.8}Ba_{0.2}NiO_2$ and Fe-d orbitals in FeSe at T = 900 K.

Five Ni-d orbitals in $La_{1-\delta}Ba_{\delta}NiO_2$ show clear spin-orbital separation. Figure 3a and c show the temperature dependence of the static local susceptibility in spin (χ^s_{tot}) and orbital (χ^o_{ij}) channels. These are defined as $\chi^s_{tot} = \sum_{ij=d}\chi^s_{ij}, \chi^s_{ij} = \int_0^\beta d\tau\langle S_{iz}(\tau)S_{jz}(0)\rangle$, and $\chi^o_{ij} = \int_0^\beta d\tau\langle N_i(\tau)N_j(0)\rangle - \beta\langle N_i\rangle\langle N_j\rangle$. Here $S_{iz}(\tau)$ is the orbital-resolved spin operator and N_i is the orbital resolved occupation operator. According to Deng et al.[91], the temperatures at which the screening of the spin and orbital degrees of freedom becomes noticeable are one of the key measures with which to distinguish between Mott and Hund physics. These onset screening temperatures in spin and orbital channels can be obtained by estimating the temperature at which these susceptibilities deviates from Curie-like behaviors. In the Mott regime, these two energy scales coincide. In contrast, in the Hund regime, the orbital onset temperature is much higher than the spin onset temperature. At a temperature between these two onset temperatures, the spin susceptibility is Curie-like but the orbital-susceptibility is Pauli-like. This is exactly the behavior seen in FeSe. In FeSe, the local spin susceptibility is Curie-like (red dots in Fig. 3a), but the local orbital susceptibility approaches its maximum upon cooling (red dots in Fig. 3c). $La_{0.8}Ba_{0.2}NiO_2$ behaves like FeSe. The spin degree of freedom (red dots in Fig. 3a) shows Curie-like behavior. In contrast, the orbital susceptibility between any Ni-d orbital pair shows a downturn of the susceptibility upon cooling (red dots in Fig. 3c).

However, there is an important distinction between the Ni-d orbitals in $La_{1-\delta}Ba_{\delta}NiO_2$ and Fe-d orbitals in FeSe: The t_{2g} orbitals in $La_{1-\delta}Ba_{\delta}NiO_2$ are inactive. In spite that Ni-t_{2g} is almost fully filled in $La_{1-\delta}Ba_{\delta}NiO_2$, the inactivity of Ni-$t_{2g}$ orbitals for the Hundness-related two-particle quantities (χ^s_{ij} and χ^o_{ij}) is a non-trivial question. Inactivity in the one-particle level (single particle Green's function) is not sufficient to assure inactivity in the two-particle level (the local susceptibilities). This can be illustrated by the charge susceptibility data obtained within multitier GW+EDMFT by F. Petocchi et al.[55]. As shown in Fig. 3 of the paper, the intraorbital charge fluctuation associated with Ni-$d_{xz/yz}$ orbitals is not negligible but comparable to the fluctuation associated with Ni-$d_{x^2-y^2}$ although Ni-$d_{xz/yz}$ orbital is almost fully-filled within their approach. To convince the inactivity of Ni-t_{2g} orbitals in the two particle level, their Hundness-related two-particle quantities (χ^s_{ij} and χ^o_{ij}) should be examined explicitly.

First, spin fluctuations are not active among the Ni-t_{2g} orbitals. Figure 3b shows χ^s_{ij}. In FeSe, all possible pairs of Fe-d orbitals show a strong spin response. In contrast, only the Ni-e_g subspace exhibits a strong spin response in $La_{0.8}Ba_{0.2}NiO_2$, while the response due to the remaining pairs is strongly suppressed. The temperature dependence of the spin susceptibility in the t_{2g} subspace ($\chi^s_{t_{2g}}$) further supports the distinction between the Ni-d orbital and Fe-d orbitals. Here, $\chi^s_{t_{2g}} = \sum_{ij=t_{2g}} \chi^s_{ij}$. As shown in Fig. 3a, $\chi^s_{t_{2g}}$ (green diamonds) in $La_{0.8}Ba_{0.2}NiO_2$ strongly deviates from the Curie-like behaviors of χ^s_{tot}. This does not occur in FeSe. Most strikingly, $\chi^s_{t_{2g}}$ approaches zero upon cooling.

Second, the static orbital susceptibility shows the suppression of orbital fluctuations in the Ni-t_{2g} subspace. Figure 3(d) shows χ^o_{ij}. In FeSe, all possible pairs of Fe-d orbitals show a strong orbital response. In contrast, the χ^o_{ij} in the Ni-t_{2g} subspace are strongly suppressed in $La_{0.8}Ba_{0.2}NiO_2$. The temperature dependence of the orbital susceptibility in the t_{2g} subspace ($\chi^o_{xy,yz}$), shown in Fig. 3c, is another distinction between Ni-d orbitals and Fe-d orbitals. Here, in contrast to FeSe, where $\chi^o_{xy,yz}$ (green diamonds) follows $\chi^o_{x^2-y^2,z^2}$ (orange squares), $\chi^o_{xy,yz}$ (green diamonds) in $La_{0.8}Ba_{0.2}NiO_2$ strongly deviates from $\chi^o_{x^2-y^2,z^2}$(orange squares). Most strikingly, $\chi^o_{xy,yz}$ approaches zero upon cooling.

Once we narrow down our view from all Ni-d orbitals into only the Ni-e_g orbitals, we can successfully find all signatures of a Hund's metal. Two Ni-e_g orbitals in $La_{1-\delta}Ba_{\delta}NiO_2$ show clear spin-orbital separation. Figure 3a and c depict the temperature dependence of static local spin ($\chi^s_{e_g}$) and orbital ($\chi^o_{x^2-y^2,z^2}$) susceptibility. Here $\chi^s_{e_g} = \sum_{ij=e_g} \chi^s_{ij}$. $\chi^s_{e_g}$ (orange squares in Fig. 3a) shows Curie-like temperature dependence but $\chi^o_{x^2-y^2,z^2}$ (orange squares in Fig. 3c) shows Pauli-like temperature dependence.

Here we note that there are two more characteristic phenomena of Hund's metal. One is the spin freezing phase[22]. At a temperature where orbital fluctuation is screened but spin flucuation is not, spin fluctuation doesn't decay to zero at long imaginary time ($\tau = \beta/2$), where β is inverse temperature. The other is orbital-decoupling: the suppression of the instantaneous interorbital charge fluctuation[11]. In these two quantities, we also found evidances of Ni-e_g Hundness. Please see the supplementary Figure 4.

Hund's physics in the infinite-layer nickelates can be tested further by measuring the temperature evolution of the Ni-$d_{x^2-y^2}$-orbital-resolved spectral function, which dominates the spectra at the Fermi level. According to Deng et al.[91], the high-temperature spectra of the orbital-resolved density of states can be used to confirm Hund's metal physics. At low temperature, spectral weight at the Fermi level is dominated by quasiparticle resonance peak in both Hund's and Mott's metallic phase. However, at a high temperature when quasiparticle spectral weight at the Fermi level are transferred to high-energy Hubbard bands, local spectra distinguish Hund-like and Mott-like metallic systems. In the metallic phase where Mott features dominate, the upper and lower Hubbard bands are well separated from each other due to its proximity to Hubbard-Mott transition and pseudo-gap forms. In contrast, in Hund's metallic phase, the upper Hubbard band is overlapping with the lower Hubbard band and the whole spectra is dominated by a single incoherent peak that has a large value at the Fermi level. This Hund's metallic features are accompanied by shoulder-like structure in the electron self-energy imaginary part as well as the inverted slope of the self-energy real part near the Fermi level[92,93].

Figure 4 shows the temperature evolution of the Ni-$d_{x^2-y^2}$-orbital-resolved spectral function of $La_{0.8}Ba_{0.2}NiO_2$. Here we note that the estimated onset screening temperature in the spin and orbital channels are 3000K and 35000K, respectively. Importantly, up to T = 15000 K, we were not able to observe pseudo gap formation in the Ni-$d_{x^2-y^2}$ projected density of states. Instead, the local spectrum is composed of a single incoherent peak that has a large value at the Fermi level. In addition, the center of the incoherent peak moves away from the Fermi-level upon heating. Furthermore, the correlation part of the electronic self-energy shows expected Hund's metallic behaviors. As shown in the self-energy in Fig. 4a there is a shoulder-like structure in its imaginary part self-energy at T = 300 K. The slope of the real part self-energy is inverted accordingly. To check its role in the spectral properties, we constructed an auxiliary Green's function of $G_{aux}(E_0, E) = \frac{1}{E-E_0-\Sigma_c(E)}$, which is often used to study Hund's metal physics in the various Hund-Hubbard models[93,94]. Due to the shoulder-like structure in the electron self-energy, the band structure of the auxiliary system is strongly renormalized with a renormalization factor of 0.2 near the Fermi level. Furthermore, at the negative bare energy (E_0), there is strong redistribution of the spectral weight, resulting in an additional incoherent peak. This creates the waterfall features in the Ni-$d_{x^2-y^2}$ orbital resolved spectral function in real materials. As shown in the spectral weight in Fig. 4a, the spectral weight along the Γ-Z line is split into strongly renormalized coherent peak and incoherent peak. As the temperature increases, the shoulder-like structure in the imaginary part of the self-energy becomes weaker. Subsequently, the coherenet and the coherent peaks merge.

To clarify the microscopic origin of Ni-e_g Hund's metallic behaviors, we investigate the reduced local many-body density or local probabilities of Ni-3d multiplet states in the atomic limit. Figure 5a shows the valence histogram for the Ni-3d multiplets in $La_{0.8}Ba_{0.2}NiO_2$. That is, it shows a partial trace of the density matrix of the full Hilbert space, where this partial trace excludes the Ni-3d subsystem in order to reveal the probability that a given multiplet state in the correlated Ni-3d subsystem is occupied. It is traced further over the secondary spin quantum number. We decompose the Ni-3d subspace according to the total charge (N_d) of the mutliplet states, and find that for $N_d = 7$, 8, 9 and 10, the most probable states involve the total spin $S_d = 1/2$, 1, 1/2, and 0 as well as the occupation of the e_g orbitals (N_{e_g}) is 1.47. 2, 3, and 4, respectively. Interestingly, these can be interpreted as the multiplets which maximize the total spin of the Ni-e_g electron in each N_{e_g} subspace; these are not the multiplets which maximize the total spin of all N-3d electrons in each N_d subspace. The reduced local many-body density on the Ni-e_g multiplets shown in Fig. 5b supports this observation. The most probable Ni-e_g multiplet in each N_{e_g} subspace is the one with maximum Ni-e_g total spin (S_{e_g}). Again, this supports our conclusion that Hund metallic behaviors are limited to the Ni-e_g orbitals.

Many-body state configurations in the Ni-e_g subshell have been discussed extensively. One of the main debates is on the spin configuration in the $Ni_{e_g} = 2$ subspace. The two holes (or

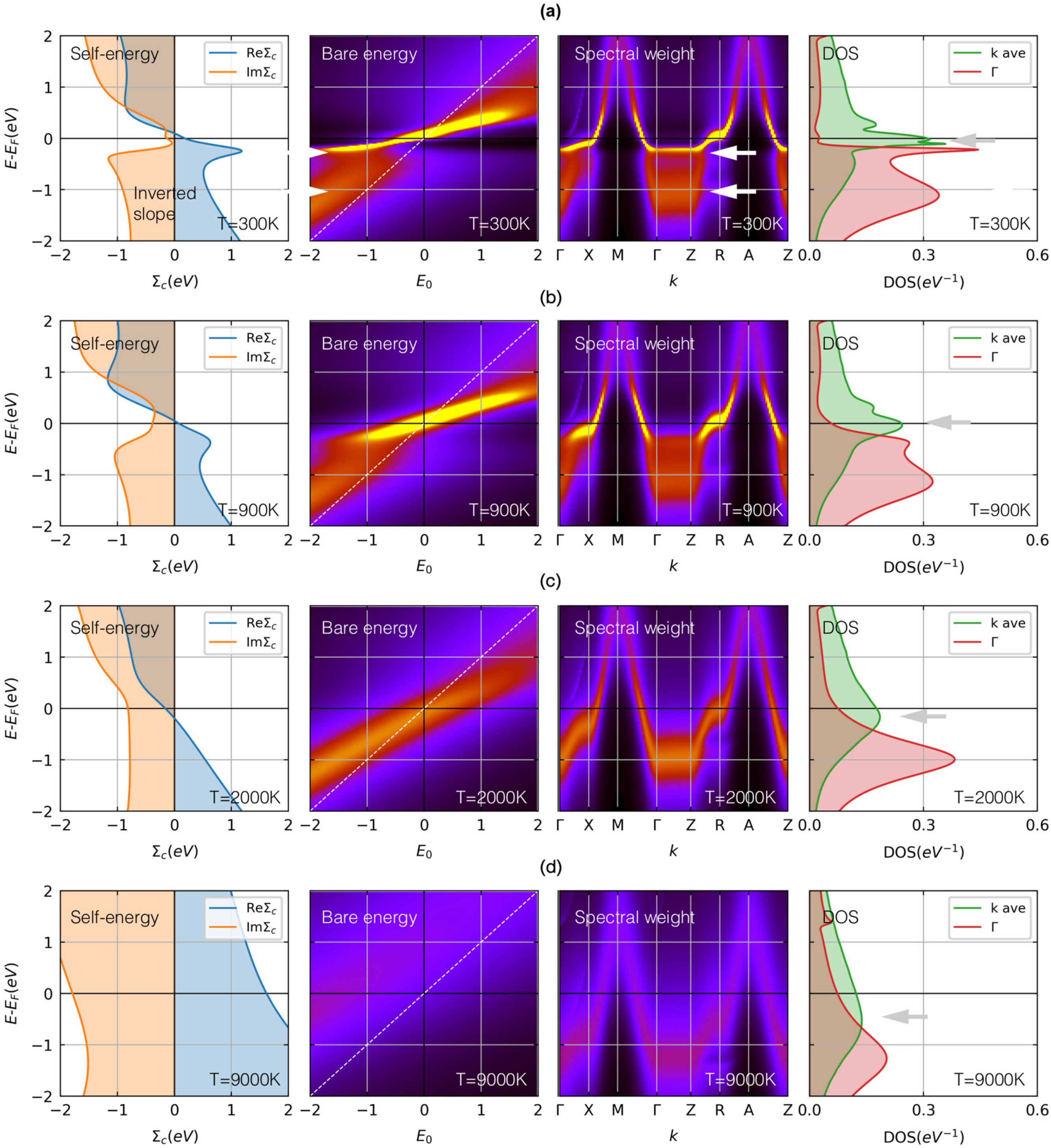

Fig. 4 Spectral functions and density of states. Spectral data obtained for Ni-$d_{x^2-y^2}$ orbital in $La_{0.8}Ba_{0.2}NiO_2$ at four different temperatures of **a** T = 300 K, **b** T = 900 K, **c** T = 2000 K, and **d** T = 9000 K. First column: electron correlation self-energy (Σ_c). Second column: spectral function of an auxiliary Green's function of $A(E_0, E) = -\frac{1}{\pi} Im\left(\frac{1}{E-E_0-\Sigma_c(E)}\right)$. White dashed line shows the dispersion of the bare band of $E = E_0$. Third column: orbital resolved spectral function. Fourth column: orbital-resolved density of states and orbital-resolved spectral function at Γ point. White arrows in the second, third and fourth columns indicate the energies of the two peaks in the orbital-resolved spectral function at the Γ point. Gray arrow in the fourth column indicates the peak in the orbital-resolved density of states.

electrons) in the Ni-e_g subspace can give rise to two different spin configurations: spin-singlet and spin-triplet. For the Ni atom in the square planar coordination environment, the competition between crystal field splitting between two Ni-e_g orbitals and Hund-coupling determines the spin configuration. Crystal field splitting favors the spin-singlet configuration[95], but Hund coupling favors the spin-triplet configuration by Hund's rule. For the infinite-layer nickelates, two different experimental studies

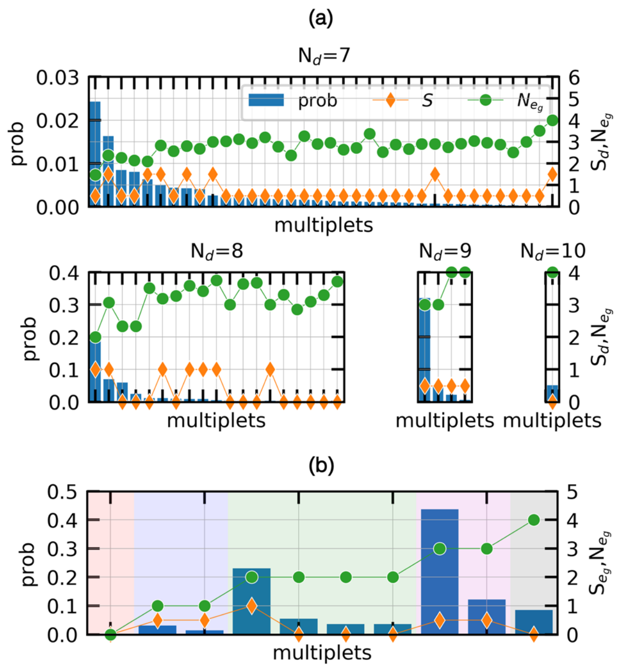

Fig. 5 Valence histograms for the Ni-3*d* multiplets. **a** Reduced local many-body density on the Ni-3*d* multiplets in $La_{0.8}Ba_{0.2}NiO_2$ at T = 300 K. Each multiplet has been labeled by using the Ni-3*d* total spin (S_d) and Ni-3*d* total charge (N_d). The Ni-e_g total charge (N_{e_g}) are also shown. **b** Reduced local many-body density on Ni-e_g multiplets in $La_{0.8}Ba_{0.2}NiO_2$ at T = 300 K. Each multiplet has been labeled by using Ni-e_g total spin (S_{e_g}), Ni-e_g total charge (N_{e_g}) and atomic-limit eigenenergy.

have been conducted on this subject. Rossi et al. reported the dominance of the singlet configuration by comparing atomic multiplet calculations with Ni L3-edge X-ray absorption spectroscopy (XAS) data of $Nd_{1-x}Sr_xNiO_2$[96]. Hepting et al. reported the dominance of the triplet configuration by comparing XAS and resonant inelastic x-ray scattering (RIXS) spectra of $LaNiO_2$ with cluster calculation[43]. Our LQSGW+DMFT data shows good agreement with Hepting et al. As shown in Fig. 5, the calculated spin-triplet and spin-singlet configurations' weights are 24% and 13%, respectively. These are very close to the values of 24% and 14% obtained by Hepting et al.[43]. The dominance of triplet configuration is one of the necessary conditions to realize Hund metal physics, and this can be an indirect evidence of the Hund metal physics in the infinite-layer nickelates.

Crystal-field splitting between Ni-e_g orbitals and two-orbital Hund metal physics

In addition to onsite Hund's coupling, the crystal-field splitting between Ni-d_{z^2} and Ni-$d_{x^2-y^2}$ orbitals is another important factor to control the physical quantities to judge Hundness versus Mottness. The crystal field splitting plays a two-faced role in those quantities. On one hand, it amplifies Hundness signatures. To illustrate, the non-zero crystal field splitting suppresses spin Kondo temperature but enhances orbital Kondo temperatures, thus boosting spin-orbital separation[94]. Thus, the spin-orbital separation in the system with a non-zero crystal-field can not be the signature of Hundness. On the other hand, it enhances Mottness signatures. The crystal field splitting makes possible Ni-e_g spin-singlet lower in energy than the spin-triplet states[97]. It also increases the separation between lower and upper Hubbard bands, thus promoting pseudo-gap formation. The enhancement of the Mottness signatures can be understood by using the Kanamori Hamiltonian in its atomic limit. By assuming inactivity

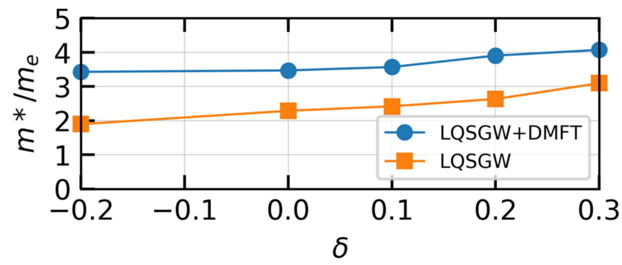

Fig. 6 Cyclotron effective mass. Doping dependence of Ni-$d_{x^2-y^2}$ band cyclotron effective mass in the $k_z = 0$ plane within LQSGW+DMFT (blue, T = 150 K) and LQSGW (orange) methods. m_e denotes the free electron mass.

Ni-t_{2g} orbitals, the local physics at the Ni site may be understood by the e_g-Kanamori Hamiltonian. In its atomic limit with vanishing intersite hopping, the Hamiltonian is given by

$$
\begin{aligned}
H = & -\Delta \sum_{\sigma} n_{2\sigma} + U \sum_{i} n_{i\uparrow} n_{i\downarrow} \\
& + \sum_{i,j,\sigma,\sigma'}^{i \neq j} \left(U' - J\delta_{\sigma,\sigma'} \right) n_{i\sigma} n_{j\sigma'} \\
& - J \sum_{i,j}^{i \neq j} \left(c_{i\uparrow}^{\dagger} c_{i\downarrow} c_{j\downarrow}^{\dagger} c_{j\uparrow} - c_{i\uparrow}^{\dagger} c_{i\downarrow}^{\dagger} c_{j\downarrow} c_{j\uparrow} \right),
\end{aligned}
\tag{1}
$$

Here, Δ, U, U' and J are the crystal-field splitting which is positive, intraorbital Coulomb interaction, interorbital Coulomb interaction, and Hund's coupling, respectively. When $\Delta = 0$, triplet states are always the lowest-energy states in $N_{e_g} = 2$ subspace. However, non-zero crystal-field splitting enables the singlet ground states formation in $N_{e_g} = 2$ subspace when $\Delta > \sqrt{(U - U' + J)^2 - J^2}$. Here we note that $U > U'$ in the realistic materials. Furthermore, the Δ promotes pseudo-gap formation by enhancing the separation between upper and lower Hubbard bands in the weakly hole-doped regime from $N_{e_g} = 3$ filling. The separation (U^{eff}) is given by $U^{eff} = U^{eff}|_{\Delta=0} + (2N_{e_g} - 5)\Delta$ when triplet states are the ground states in $N_{e_g} = 2$ subspace and $U^{eff} = U^{eff}|_{\Delta=0} + (2N_{e_g} - 5)\Delta - (3N_{e_g} - 8)(\sqrt{J^2 + \Delta^2} - J)$ when a singlet is the ground state in $N_{e_g} = 2$ subspace. Here $U^{eff}|_{\Delta=0}$ is the energy gap when Δ=0. $U^{eff} \geq U^{eff}|_{\Delta=0}$ in the electron occupation of $2.5 < N_{e_g} < 3$ regardless of $N_{e_g} = 2$ subspace ground state. For the derivation, please see the Supplementary Table 2.

Despite the crystal-field-induced enhancement of the pseudo-gap as well as singlet population, both measures advocate Hund's metallicity of $La_{1-\delta}Ba_{\delta}NiO_2$ as shown in Figs. 5b and 4. Together with the spin-orbital separation shown in Fig. 3, these signatures indicate that $La_{1-\delta}Ba_{\delta}NiO_2$ is a strong candidate of two-orbital Hund's metal.

Measuring the two-orbital Hundness experimentally

We propose another experiment to support Ni-e_g Hundness in the infinite-layer nickelates: the doping dependence of Ni-$d_{x^2-y^2}$ band effective mass. In a paramagnetic system where the proximity to Mott transition dominates electron correlation and single-band is a good minimum model to describe the low-energy physics, the effective mass is expected to be maximum in the undoped system and decreases if the system is either hole-doped or electron-doped. In contrast, as demonstrated by the Fe-based superconductors[98], the effective mass of Hund's metals changes monotonically from hole-doped side to electron-doped side in Hund's metals. Figure 6 shows the doping dependence of the cyclotron effective mass of the Ni-$d_{x^2-y^2}$ bands in the $k_z = 0$ plane. Both LQSGW+DMFT and LQSGW methods show that the effective mass increases monotonically from electron doped side

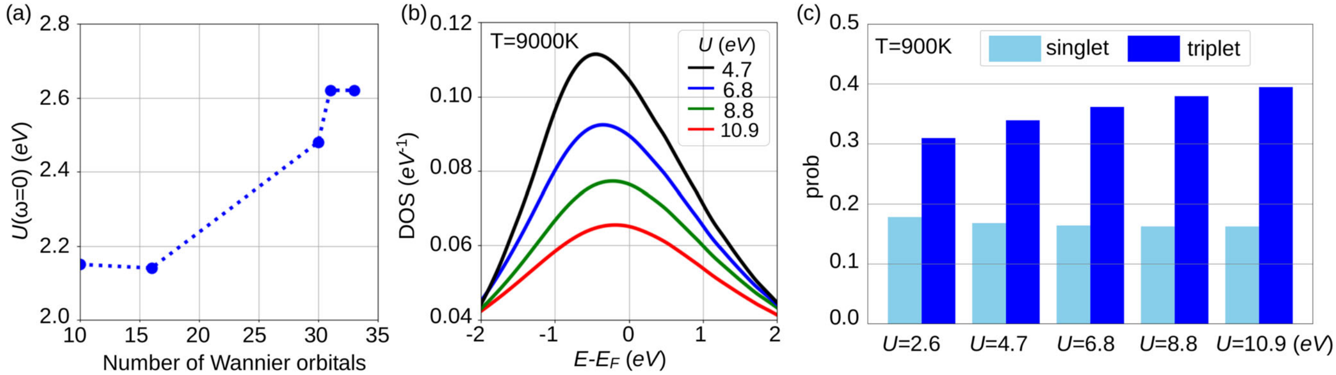

Fig. 7 ***U* and Hund physics in the infinite-layer nickelates.** **a** Calculated static on-site Coulomb interaction $U(\omega = 0)$ as a function of the number of Wannier orbitals. **b** Projected density of states for Ni-$d_{x^2-y^2}$ orbital in $La_{0.8}Ba_{0.2}NiO_2$ at T = 9000 K, as a function of *U*. Each line is labeled by the static value of *U*. **c** Calculated spin-triplet and spin-singlet configurations' weights at T = 900 K, as a function of *U*.

to hole-doped side. This monotonic doping dependence of the effective mass could be confimed by other experiments such as specific heat measurement as well as angle-resolved photoemission spectroscopy. In contrast to other signatures proposed in this paper, the doping dependence of the Ni-$d_{x^2-y^2}$ band effective mass does not require high temperature measurements.

Hubbard U and Hund metal physics in the infinite-layer nickelates

We calculated the Slater integral $F_0 = 2.56$, $F_2 = 8.50$, and $F_4 = 6.69$ eV within cRPA. Then, we parameterized static $U = F_0$ and $J = (F_2 + F_4)/14$ having $U = 2.56$ and $J = 1.09$ eV. We compared our static *U* and *J* with the results from Sakakibara et al.[53], who employed different parametrization of $U_{d_{x^2-y^2}}$=$(F_0 + (F_2 + F_4)4/49)$, $J = (F_2 + F_4)5/98$, and U'=$U_{d_{x^2-y^2}}$-$(J)8/5$. Using our $F_0 = 2.56$, $F_2 = 8.50$, and $F_4 = 6.69$ eV for the parametrization, we found $U_{d_{x^2-y^2}}$=3.8, $J = 0.775$, and U'=2.56 eV, which are almost the same as $U_{d_{x^2-y^2}}$=3.81, $J = 0.71$, and U'=2.62 eV from Sakakibara et al. However, Sakakibara et al. employed a seven-orbital model[53], whereas we used 31 Wannier functions including O-*p* orbitals. Moreover, a wide range of *U* values from 2.6 to 5.3 eV have been reported for a number of orbitals ranging from 2 to 7[53,55,87]. Thus, our relatively small *U* using 31 orbitals is not consistent with the previous results. The inconsistency in *U* is an important future research topic.

First, we checked the convergence of the *U* obtained by cRPA, as a function of the number of orbitals which is determined by the Wannier frozen-energy window. As shown in Fig. 7a, the static *U* increases and saturates at 2.63 eV (3.87 eV with the different parameterization) as the number of orbitals increases. However, it does not reach 5.3 eV from the 7 orbital model[55].

Then we tested the effect of *U* on the Hundness in the infinite-layer nickelate. We intentionally increased dynamical part of *U* and checked the evolution of Ni-$d_{x^2-y^2}$ PDOS and local many-body density. Figure 7b shows PDOS of Ni-$d_{x^2-y^2}$ at T = 9000 K. When we increase the dynamical part of *U*, Ni-$d_{x^2-y^2}$ occupation deviates further from the half-filling and the line shape of the Ni-$d_{x^2-y^2}$ DOS still shows a single incoherent peak without pseudo gap. This suggests no significant effect of *U* on the Hundness in the infinite-layer nickelates. Figure 7c shows the calculated weights of the spin-triplet and spin-singlet configurations as a function of the dynamical *U*. The dominance of triplet configuration over all *U* indicates the minor role of *U* on the origin of correlated metallic phase. These results suggest that *U* is not a dominant factor in the electronic structure of the infinite-layer nickelates and support support Hund metal physics in the infinite-layer nickelates.

In conclusion, by using ab initio LQSGW+DMFT methodology, we demonstrated that on-site Hund's coupling in Ni-*d* orbitals results in multiple signatures of Hund's metallic phase in Ni-e_g orbitals. Our finding sheds a light on Hundness in the correlated quantum materials and has potential implications for the broad range of correlated two orbital systems away from half-filling and the role of on-site Hund's coupling[11,50,99].

METHODS

LQSGW and DMFT calculations

Following the literature[34,43,53,54,79,86,88,100], we studied $La_{1-\delta}Ba_{\delta}NiO_2$ instead of $Nd_{1-\delta}Sr_{\delta}NiO_2$ to avoid the difficulty in the treatment of the Nd-4*f* band. This is acceptable, as it has been reported that $LaNiO_2$ at the lattice parameters of $NdNiO_2$ has a similar electronic structure of $NdNiO_2$ within open Nd-*f* core approximation[34]. It has been experimentally demonstrated that the Nd-4*f* states of Nd-based infinite layer nickelates are well localized and do not influence the relevant physics close to the Fermi level[43,96]. The effect of Ba doping has been treated within the virtual crystal approximation. For its justification, please see the supplementary methods. For the LQSGW+DMFT scheme, the code ComDMFT[58] was used. For the LQSGW part of the LQSGW+DMFT scheme, the code FlapwMBPT[63] was used. For the details of electronic structure calculation, please see the supplementary methods.

DATA AVAILABILITY

The data that support the findings of this study are available from the corresponding authors upon reasonable request.

Received: 20 July 2022; Accepted: 30 June 2023;
Published online: 12 July 2023

REFERENCES

1. Bednorz, J. G. & Müller, K. A. Possible high T_c superconductivity in the Ba-La-Cu-O system. *Z. Phys. B* **64**, 189–193 (1986).
2. Zaanen, J., Sawatzky, G. A. & Allen, J. W. Band gaps and electronic structure of transition-metal compounds. *Phys. Rev. Lett.* **55**, 418–421 (1985).
3. Mott, N. F. & Peierls, R. Discussion of the paper by de Boer and Verwey. *Proc. Phys. Soc.* **49**, 72 (1937).
4. Mott, N. F. The basis of the electron theory of metals, with special reference to the transition metals. *Proc. Phys. Soc. A* **62**, 416–422 (1949).
5. Lee, P. A., Nagaosa, N. & Wen, X.-G. Doping a Mott insulator: Physics of high-temperature superconductivity. *Rev. Mod. Phys.* **78**, 17–85 (2006).
6. Garg, A., Randeria, M. & Trivedi, N. Strong correlations make high-temperature superconductors robust against disorder. *Nat. Phys.* **4**, 762–765 (2008).
7. Keimer, B., Kivelson, S. A., Norman, M. R., Uchida, S. & Zaanen, J. From quantum matter to high-temperature superconductivity in copper oxides. *Nature* **518**, 179–186 (2015).

8. Kamihara, Y. et al. Iron-based layered superconductor: LaOFeP. *J. Am. Chem. Soc.* **128**, 10012–10013 (2006).
9. Kamihara, Y., Watanabe, T., Hirano, M. & Hosono, H. Iron-based layered superconductor $La[O_{1-x}F_x]FeAs$ (x = 0.05 - 0.12) with T_c = 26 K. *J. Am. Chem. Soc.* **130**, 3296–3297 (2008).
10. de' Medici, L., Mravlje, J. & Georges, A. Janus-faced influence of Hund's rule coupling in strongly correlated materials. *Phys. Rev. Lett.* **107**, 256401 (2011).
11. de'Medici, L. Hund's coupling and its key role in tuning multiorbital correlations. *Phys. Rev. B* **83**, 205112 (2011).
12. Georges, A., Medici, L. D. & Mravlje, J. Strong correlations from Hund's coupling. *Annu. Rev. Condens. Matter Phys.* **4**, 137–178 (2013).
13. Isidori, A. et al. Charge disproportionation, mixed valence, and Janus effect in multiorbital systems: A tale of two insulators. *Phys. Rev. Lett.* **122**, 186401 (2019).
14. Haule, K. & Kotliar, G. Coherence-incoherence crossover in the normal state of iron oxypnictides and importance of Hund's rule coupling. *New J. Phys.* **11**, 025021 (2009).
15. Yin, Z. P., Haule, K. & Kotliar, G. Kinetic frustration and the nature of the magnetic and paramagnetic states in iron pnictides and iron chalcogenides. *Nat. Mater.* **10**, 932–935 (2011).
16. Chibani, S. et al. Lattice-shifted nematic quantum critical point in $FeSe_{1-x}S_x$. *npj Quantum Mater.* **6**, 37 (2021).
17. de' Medici, L. Hund's induced Fermi-liquid instabilities and enhanced quasiparticle interactions. *Phys. Rev. Lett.* **118**, 167003 (2017).
18. Lanatà, N. et al. Orbital selectivity in Hund's metals: the iron chalcogenides. *Phys. Rev. B* **87**, 045122 (2013).
19. Villar Arribi, P. & de' Medici, L. Hund-enhanced electronic compressibility in fese and its correlation with T_c. *Phys. Rev. Lett.* **121**, 197001 (2018).
20. Bascones, E., Valenzuela, B. & Calderón, M. J. Orbital differentiation and the role of orbital ordering in the magnetic state of Fe superconductors. *Phys. Rev. B* **86**, 174508 (2012).
21. Ryee, S., Sémon, P., Han, M. J. & Choi, S. Nonlocal Coulomb interaction and spin-freezing crossover as a route to valence-skipping charge order. *npj Quantum Mater.* **5**, 1–6 (2020).
22. Werner, P., Gull, E., Troyer, M. & Millis, A. J. Spin freezing transition and non-Fermi-liquid self-energy in a three-orbital model. *Phys. Rev. Lett.* **101**, 166405 (2008).
23. Mravlje, J. et al. Coherence-incoherence crossover and the mass-renormalization puzzles in Sr_2RuO_4. *Phys. Rev. Lett.* **106**, 096401 (2011).
24. Hoshino, S. & Werner, P. Superconductivity from emerging magnetic moments. *Phys. Rev. Lett.* **115**, 247001 (2015).
25. Mravlje, J. & Georges, A. Thermopower and entropy: lessons from Sr_2RuO_4. *Phys. Rev. Lett.* **117**, 036401 (2016).
26. Li, D. et al. Superconductivity in an infinite-layer nickelate. *Nature* **572**, 624–627 (2019).
27. Li, D. et al. Superconducting dome in $Nd_{1-x}Sr_xNiO_2$ infinite layer films. *Phys. Rev. Lett.* **125**, 027001 (2020).
28. Gu, Q. et al. Two superconducting components with different symmetries in $Nd_{1-x}Sr_xNiO_2$ films. Preprint at http://arxiv.org/abs/2006.13123 (2020).
29. Zeng, S. et al. Phase diagram and superconducting dome of infinite-layer $Nd_{1-x}Sr_xNiO_2$ thin films. *Phys. Rev. Lett.* **125**, 147003 (2020).
30. Sawatzky, G. A. Superconductivity seen in a non-magnetic nickel oxide. *Nature* **572**, 592–593 (2019).
31. Xiang, Y. et al. Magnetic transport properties of superconducting $Nd_{1-x}Sr_xNiO_2$ thin films. Preprint at http://arxiv.org/abs/2007.04884 (2020).
32. Hayward, M. A., Green, M. A., Rosseinsky, M. J. & Sloan, J. Sodium hydride as a powerful reducing agent for topotactic oxide deintercalation: synthesis and characterization of the nickel (I) oxide $LaNiO_2$. *J. Am. Chem. Soc.* **121**, 8843–8854 (1999).
33. Hayward, M. A. & Rosseinsky, M. J. Synthesis of the infinite layer Ni(I) phase $NdNiO_{2+x}$ by low temperature reduction of $NdNiO_3$ with sodium hydride. *Solid State Sci.* **5**, 839–850 (2003).
34. Botana, A. & Norman, M. Similarities and differences between $LaNiO_2$ and $CaCuO_2$ and implications for superconductivity. *Phys. Rev. X* **10**, 011024 (2020).
35. Kitatani, M. et al. Nickelate superconductors-a renaissance of the one-band Hubbard model. *npj Quantum Mater.* **5**, 1–6 (2020).
36. Hirsch, J. E. & Marsiglio, F. Hole superconductivity in infinite-layer nickelates. *Physica C* **566**, 1353534 (2019).
37. Wu, X. et al. Robust $d_{x^2-y^2}$-wave superconductivity of infinite-layer nickelates. *Phys. Rev. B* **101**, 060504 (2020).
38. Karp, J. et al. Many-body electronic structure of $NdNiO_2$ and $CaCuO_2$. *Phys. Rev. X* **10**, 021061 (2020).
39. Lang, Z.-J., Jiang, R. & Ku, W. et al. Strongly correlated doped hole carriers in the superconducting nickelates: their location, local many-body state, and low-energy effective hamiltonian. *Phys. Rev. B* **103**, L180502 (2021).
40. Ikeda, A., Manabe, T. & Naito, M. Improved conductivity of infinite-layer $LaNiO_2$ thin films by metal organic decomposition. *Phys. C* **495**, 134–140 (2013).
41. Ikeda, A., Krockenberger, Y., Irie, H., Naito, M. & Yamamoto, H. Direct observation of infinite NiO_2 planes in $LaNiO_2$ films. *Appl. Phys. Exp.* **9**, 061101 (2016).
42. Fu, Y. et al. Electronic structures and spin fluctuations in nickelate oxide $NdNiO_2$. Preprint at http://arxiv.org/abs/1911.03177 (2019).
43. Hepting, M. et al. Electronic structure of the parent compound of superconducting infinite-layer nickelates. *Nat. Mater.* **19**, 381–385 (2020).
44. Lechermann, F. Multiorbital processes rule the $Nd_{1-x}Sr_xNiO_2$ normal state. *Phys. Rev. X* **10**, 041002 (2020).
45. Adhikary, P., Bandyopadhyay, S., Das, T., Dasgupta, I. & Saha-Dasgupta, T. Orbital-selective superconductivity in a two-band model of infinite-layer nickelates. *Phys. Rev. B* **102**, 100501 (2020).
46. Goodge, B. H. et al. Doping evolution of the mott–hubbard landscape in infinite-layer nickelates. *PNAS* **118**, e2007683118 (2021).
47. Jiang, M., Berciu, M. & Sawatzky, G. A. Critical nature of the Ni spin state in doped $NdNiO_2$. *Phys. Rev. Lett.* **124**, 207004 (2020).
48. Zhang, Y.-H. & Vishwanath, A. Type-II *t-J* model in superconducting nickelate $Nd_{1-x}Sr_xNiO_2$. *Phys. Rev. Res.* **2**, 023112 (2020).
49. Hu, L.-H. & Wu, C. Two-band model for magnetism and superconductivity in nickelates. *Phys. Rev. Res.* **1**, 032046 (2019).
50. Werner, P. & Hoshino, S. Nickelate superconductors: multiorbital nature and spin freezing. *Phys. Rev. B* **101**, 041104 (2020).
51. Zhang, G.-M., Yang, Y.-f & Zhang, F.-C. Self-doped Mott insulator for parent compounds of nickelate superconductors. *Phys. Rev. B* **101**, 020501 (2020).
52. Chang, J., Zhao, J. & Ding, Y. Hund-heisenberg model in superconducting infinite-layer nickelates. *Eur. Phys. J. B* **93**, 1–7 (2020).
53. Sakakibara, H. et al. Model construction and a possibility of cupratelike pairing in a new d^9 nickelate superconductor (Nd,Sr)NiO_2. *Phys. Rev. Lett.* **125**, 077003 (2020).
54. Wang, Y., Kang, C.-J., Miao, H. & Kotliar, G. Hund's metal physics: from $SrNiO_2$ to $LaNiO_2$. *Phys. Rev. B* **102**, 161118 (2020).
55. Petocchi, F., Christiansson, V., Nilsson, F., Aryasetiawan, F. & Werner, P. Normal state of $Nd_{1-x}Sr_xNiO_2$ from self-consistent *GW*+EDMFT. *Phys. Rev. X* **10**, 041047 (2020).
56. Tomczak, J. M. QSGW +DMFT: an electronic structure scheme for the iron pnictides and beyond. *J. Phys.: Conf. Ser.* **592**, 012055 (2015).
57. Choi, S., Kutepov, A., Haule, K., van Schilfgaarde, M. & Kotliar, G. First-principles treatment of Mott insulators: linearized QSGW+DMFT approach. *npj Quan. Mater.* **1**, 16001 (2016).
58. Choi, S., Semon, P., Kang, B., Kutepov, A. & Kotliar, G. ComDMFT: a massively parallel computer package for the electronic structure of correlated-electron systems. *Comput. Phys. Commun.* **244**, 277–294 (2019).
59. Sun, P. & Kotliar, G. Extended dynamical mean-field theory and GW method. *Phys. Rev. B* **66**, 085120 (2002).
60. Biermann, S., Aryasetiawan, F. & Georges, A. First-principles approach to the electronic structure of strongly correlated systems: combining the GW approximation and dynamical mean-field theory. *Phys. Rev. Lett.* **90**, 086402 (2003).
61. Nilsson, F., Boehnke, L., Werner, P. & Aryasetiawan, F. Multitier self-consistent *GW* +EDMFT. *Phys. Rev. Mater.* **1**, 043803 (2017).
62. Kutepov, A., Haule, K., Savrasov, S. Y. & Kotliar, G. Electronic structure of Pu and Am metals by self-consistent relativistic GW method. *Phys. Rev. B* **85**, 155129 (2012).
63. Kutepov, A., Oudovenko, V. & Kotliar, G. Linearized self-consistent quasiparticle GW method: application to semiconductors and simple metals. *Comput. Phys. Commun.* **219**, 407–414 (2017).
64. Georges, A., Kotliar, G., Krauth, W. & Rozenberg, M. J. Dynamical mean-field theory of strongly correlated fermion systems and the limit of infinite dimensions. *Rev. Mod. Phys.* **68**, 13–125 (1996).
65. Metzner, W. & Vollhardt, D. Correlated lattice Fermions in $d=\infty$ dimensions. *Phys. Rev. Lett.* **62**, 324–327 (1989).
66. Müller-Hartmann, E. Correlated fermions on a lattice in high dimensions. *Z. Phys. B* **74**, 507–512 (1989).
67. Brandt, U. & Mielsch, C. Thermodynamics and correlation functions of the Falicov-Kimball model in large dimensions. *Z. Phys. B* **75**, 365–370 (1989).
68. Janiš, V. A new construction of thermodynamic mean-field theories of itinerant fermions: application to the Falicov-Kimball model. *Z. Phys. B* **83**, 227–235 (1991).
69. Georges, A. & Kotliar, G. Hubbard model in infinite dimensions. *Phys. Rev. B* **45**, 6479–6483 (1992).
70. Jarrell, M. Hubbard model in infinite dimensions: a quantum Monte Carlo study. *Phys. Rev. Lett.* **69**, 168–171 (1992).
71. Rozenberg, M. J., Zhang, X. Y. & Kotliar, G. Mott-Hubbard transition in infinite dimensions. *Phys. Rev. Lett.* **69**, 1236–1239 (1992).
72. Georges, A. & Krauth, W. Numerical solution of the $d=\infty$ Hubbard model: evidence for a Mott transition. *Phys. Rev. Lett.* **69**, 1240–1243 (1992).

73. Aryasetiawan, F. et al. Frequency-dependent local interactions and low-energy effective models from electronic structure calculations. *Phys. Rev. B* **70**, 195104 (2004).
74. Chikina, A. et al. Correlated electronic structure of colossal thermopower $FeSb_2$: an ARPES and *abinitio* study. *Phys. Rev. Res.* **2**, 023190 (2020).
75. Siddiquee, H. et al. Breakdown of the scaling relation of anomalous Hall effect in Kondo lattice ferromagnet USbTe. *Nat. Commun.* **14**, 527 (2023).
76. Kang, B., Lee, Y., Ke, L., Kim, H. & Kim, M.-H. Dual nature of magnetism driven by momentum dependent *f-d* Kondo hybridization. *arXiv preprint arXiv:2305.08003* (2023).
77. Kang, B., Choi, S. & Kim, H. Orbital selective Kondo effect in heavy fermion superconductor UTe_2. *npj Quantum Mater.* **7**, 64 (2022).
78. Kang, B., Kim, H., Zhu, Q. & Park, C. H. Impact of *f-d* Kondo cloud on superconductivity of nickelates. *Cell Rep. Phys. Sci.* **4**, 101325 (2023).
79. Bernardini, F., Olevano, V. & Cano, A. Magnetic penetration depth and T_c in superconducting nickelates. *Phys. Rev. Res.* **2**, 013219 (2020).
80. Jiang, P., Si, L., Liao, Z. & Zhong, Z. Electronic structure of rare-earth infinite-layer $RNiO_2$ (R=La,Nd). *Phys. Rev. B* **100**, 201106 (2019).
81. Lechermann, F. Late transition metal oxides with infinite-layer structure: nickelates versus cuprates. *Phys. Rev. B* **101**, 081110 (2020).
82. Lee, K.-W. & Pickett, W. E. Infinite-layer $LaNiO_2$: Ni^{1+} is not Cu^{2+}. *Phys. Rev. B* **70**, 165109 (2004).
83. Zhang, H. et al. Effective Hamiltonian for nickelate oxides $Nd_{1-x}Sr_xNiO_2$. *Phys. Rev Res.* **2**, 013214 (2020).
84. Been, E. et al. Electronic structure trends across the rare-earth series in superconducting Infinite-Layer nickelates. *Phys. Rev. X* **11**, 011050 (2021).
85. Gu, Y., Zhu, S., Wang, X., Hu, J. & Chen, H. A substantial hybridization between correlated Ni-*d* orbital and itinerant electrons in infinite-layer nickelates. *Commun. Phys.* **3**, 1–9 (2020).
86. Olevano, V., Bernardini, F., Blase, X. & Cano, A. Ab initio many-body GW correlations in the electronic structure of $LaNiO_2$. *Phys. Rev. B* **101**, 161102 (2020).
87. Nomura, Y. et al. Formation of a two-dimensional single-component correlated electron system and band engineering in the nickelate superconductor $NdNiO_2$. *Phys. Rev. B* **100**, 205138 (2019).
88. Leonov, I., Skornyakov, S. L. & Savrasov, S. Y. Lifshitz transition and frustration of magnetic moments in infinite-layer $NdNiO_2$ upon hole doping. *Phys. Rev. B* **101**, 241108 (2020).
89. Choi, M.-Y., Pickett, W. E. & Lee, K.-W. Fluctuation-frustrated flat band instabilities in $NdNiO_2$. *Phys. Rev. Res.* **2**, 033445 (2020).
90. Ryee, S., Han, M. J. & Choi, S. Hund physics landscape of two-orbital systems. *Phys. Rev. Lett.* **126**, 206401 (2021).
91. Deng, X. et al. Signatures of Mottness and Hundness in archetypal correlated metals. *Nat. Commun.* **10**, 2721 (2019).
92. Stadler, K., Yin, Z., von Delft, J., Kotliar, G. & Weichselbaum, A. Dynamical mean-field theory plus numerical renormalization-group study of spin-orbital separation in a three-band Hund metal. *Phys. Rev. Lett.* **115**, 136401 (2015).
93. Stadler, K. M., Kotliar, G., Weichselbaum, A. & von Delft, J. Hundness versus Mottness in a three-band Hubbard-Hund model: on the origin of strong correlations in Hund metals. *Ann. Phys.* **405**, 365–409 (2019).
94. Kugler, F. B., Lee, S.-S. B., Weichselbaum, A., Kotliar, G. & von Delft, J. Orbital differentiation in Hund metals. *Phys. Rev. B* **100**, 115159 (2019).
95. Matsumoto, Y. et al. High-pressure synthesis of $A_2NiO_2Ag_2Se_2$ (A= Sr, Ba) with a high-spin Ni^{2+} in square-planar coordination. *Angew. Chem. Int. Ed.* **58**, 756–759 (2019).
96. Rossi, M. et al. Orbital and spin character of doped carriers in infinite-layer nickelates. *Phys. Rev. B* **104**, L220505 (2021).
97. Werner, P. & Millis, A. J. High-spin to low-spin and orbital polarization transitions in multiorbital Mott systems. *Phys. Rev. Lett.* **99**, 126405 (2007).
98. de' Medici, L., Giovannetti, G. & Capone, M. Selective Mott physics as a key to iron superconductors. *Phys. Rev. Lett.* **112**, 177001 (2014).
99. Stadler, K. M.A model study of strong correlations in Hund metals. PhD Thesis. (Ludwig-Maximilians-Universität München, 2019).
100. Ryee, S., Yoon, H., Kim, T. J., Jeong, M. Y. & Han, M. J. Induced magnetic two-dimensionality by hole doping in the superconducting infinite-layer nickelate $Nd_{1-x}Sr_xNiO_2$. *Phys. Rev. B* **101**, 064513 (2020).

ACKNOWLEDGEMENTS

S.C. thanks G. L. Pascut, and C-.J-. Kang and for useful conversation. This work was supported by the U.S Department of Energy, Office of Science, Basic Energy Sciences as a part of the Computational Materials Science Program. S.C. was supported by a KIAS individual Grant (No. CG090601) at Korea Institute for Advanced Study. S. R and M. J. H were supported by NRF Korea (2018R1A2B2005204 and 2018M3D1A1058754). This research used resources of the National Energy Research Scientific Computing Center (NERSC), a U.S. Department of Energy Office of Science User Facility operated under Contract No. DE-AC02-05CH11231.

AUTHOR CONTRIBUTIONS

S.C. conceived the project. B.K. performed all calculations. C.M. modified ComCTQMC solver to print out local many-body density matrices. B.K., S.R., M.J.H, G.K, and S.C. discussed the data and wrote the manuscript. All authors commented on the document.

COMPETING INTERESTS

The authors declare no competing interests.

ADDITIONAL INFORMATION

Supplementary information The online version contains supplementary material available at https://doi.org/10.1038/s41535-023-00568-5.

Correspondence and requests for materials should be addressed to Sangkook Choi.

Reprints and permission information is available at http://www.nature.com/reprints

Publisher's note Springer Nature remains neutral with regard to jurisdictional claims in published maps and institutional affiliations.